



Comparison of impervious surface area and normalized difference vegetation index as indicators of surface urban heat island effects in Landsat imagery

Fei Yuan ^{a,*}, Marvin E. Bauer ^b

^a *Minnesota State University – Mankato, Department of Geography, Mankato, Minnesota 56001, United States*

^b *University of Minnesota, Department of Forest Resources, 1530 Cleveland Avenue North, St. Paul, Minnesota 55108, United States*

Received 5 June 2006; received in revised form 5 September 2006; accepted 7 September 2006

Abstract

This paper compares the normalized difference vegetation index (NDVI) and percent impervious surface as indicators of surface urban heat island effects in Landsat imagery by investigating the relationships between the land surface temperature (LST), percent impervious surface area (%ISA), and the NDVI. Landsat Thematic Mapper (TM) and Enhanced Thematic Mapper Plus (ETM+) data were used to estimate the LST from four different seasons for the Twin Cities, Minnesota, metropolitan area. A map of percent impervious surface with a standard error of 7.95% was generated using a normalized spectral mixture analysis of July 2002 Landsat TM imagery. Our analysis indicates there is a strong linear relationship between LST and percent impervious surface for all seasons, whereas the relationship between LST and NDVI is much less strong and varies by season. This result suggests percent impervious surface provides a complementary metric to the traditionally applied NDVI for analyzing LST quantitatively over the seasons for surface urban heat island studies using thermal infrared remote sensing in an urbanized environment.

© 2006 Elsevier Inc. All rights reserved.

Keywords: Impervious surface area; Land surface temperature; Normalized difference vegetation index; Spectral mixture analysis; Surface urban heat island; Landsat TM/ETM+

1. Introduction

The urban heat island (UHI) refers to the phenomenon of higher atmospheric and surface temperatures occurring in urban areas than in the surrounding rural areas due to urbanization (Voogt & Oke, 2003). It is characterized by a large expanse of non-evaporating impervious materials covering a majority of urban areas with a consequent increase in sensible heat flux at the expense of latent heat flux (Oke, 1982; Owen et al., 1998). UHI effects are exacerbated by the anthropogenic heat generated by traffic, industry and domestic buildings, impacting the local climate through the city's compact mass of buildings that affect exchange of energy and levels of conductivity. The higher temperatures in urban heat islands increase air conditioning demands, raise pollution levels, and may modify precipitation patterns. As a result, the

magnitude and pattern of UHI effects have been major concerns of many urban climatology studies.

Heat islands can be characterized for different layers of the urban atmosphere and for various surfaces and divided into three categories: canopy layer heat island (CLHI), boundary layer heat island (BLHI), and surface urban heat island (SUHI). The urban canopy layer extends upwards from the surface to approximately mean building height, whereas the urban boundary layer is located above the canopy layer (Voogt & Oke, 2003). The CLHI and the BLHI are atmospheric heat islands since they denote a warming of the urban atmosphere, whereas the SUHI refers to the relative warmth of urban surfaces compared to surrounding rural areas. It is known that atmospheric UHIs are larger at night while surface UHIs are larger during the day (Roth et al, 1989). While atmospheric heat islands are normally measured by in situ sensors of air temperature via weather station networks, the surface UHI is typically characterized as land surface temperature (LST) through the use of airborne or satellite thermal infrared remote sensing, which provides a synoptic and uniform means of

* Corresponding author. Tel.: +1 507 389 2376; fax: +1 507 389 2980.

E-mail address: fei.yuan@mnsu.edu (F. Yuan).

studying SUHI effects at regional scales. Satellite-measured LST has been utilized in various heat-balance, climate modeling, and global-change studies since it is determined by the effective radiating temperature of the Earth's surface, which controls surface heat and water exchange with the atmosphere. Voogt and Oke (2003) suggested three major applications of thermal remote sensing to the study of urban climates. Two of them focus on examining relations either between spatial structure of urban thermal patterns and urban surface characteristics or between atmospheric and surface heat islands; the third is centered on studying urban surface energy balances by coupling urban climate models with remotely sensed data. Our study addresses the first application area.

In earlier thermal remote sensing studies, much emphasis has been placed on using the normalized difference vegetation index (NDVI) as the major indicator of urban climate. For example, Gallo et al. (1993) assessed the influence of the urban

environment on observed minimum air temperatures by analyzing urban–rural differences for NDVI and surface temperatures. Lo et al. (1997) studied changes in the thermal responses of urban land cover types between day and night and examined the relation between land cover radiance and vegetation amount using NDVI derived from Advanced Thermal and Land Applications Sensor (ATLAS) data. Gallo and Owen (1999) evaluated seasonal trends in temperature and NDVI and found that differences in NDVI and satellite-based surface temperature accounted for 40% of the variation in urban–rural temperature differences. The NDVI–temperature relationship has also been utilized in various studies to derive or evaluate two variables — fractional vegetation cover and surface soil water content for climate modeling (Carlson et al., 1995a; Gillies & Carlson, 1995; Gillies et al., 1997; Goward et al., 2002).

Higher NDVI values typically indicate a larger fraction of vegetation in a pixel. The amount of vegetation determines

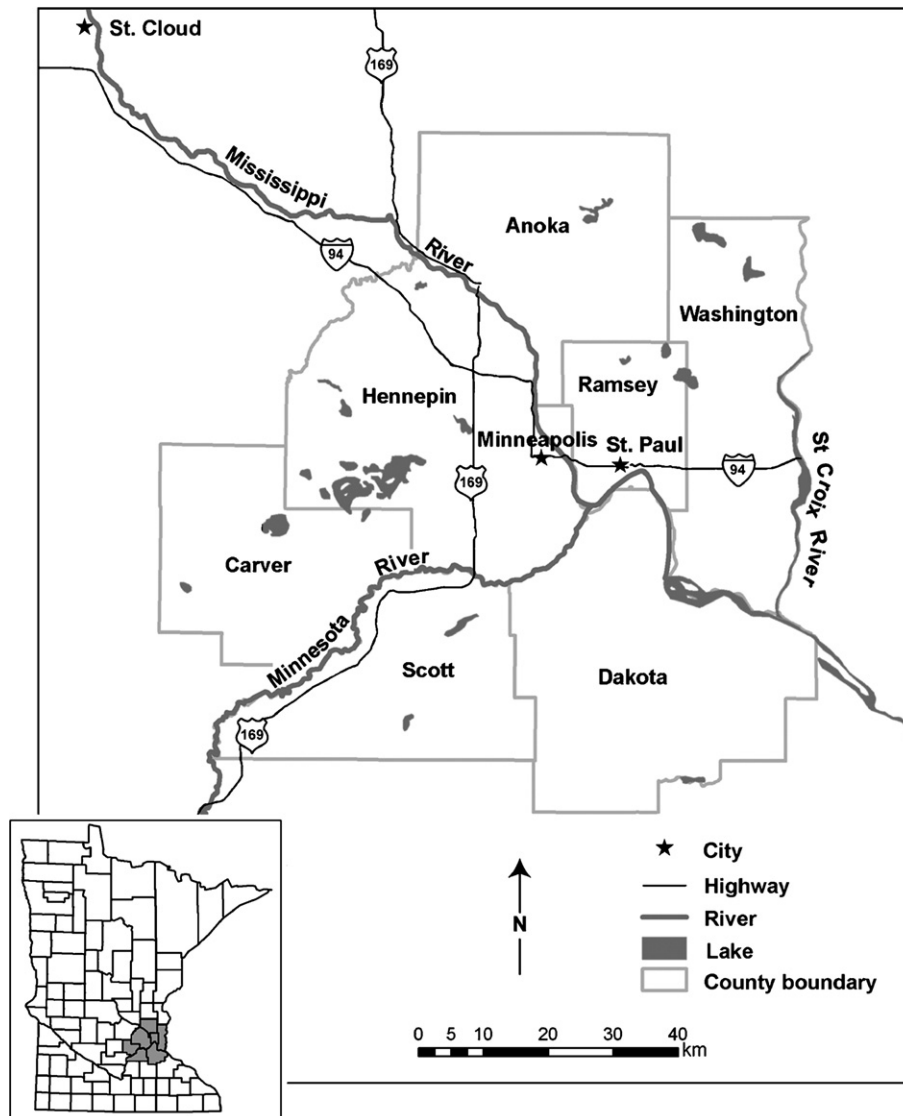


Fig. 1. Seven-county Twin Cities Metropolitan Area (TCMA) of Minnesota.

LST by the latent heat flux from the surface to atmosphere via evapotranspiration. Lower LSTs usually are found in areas with high NDVI. This negative correlation between NDVI and LST is valuable for urban climate studies. However, NDVI measurements are subject to seasonal variations which may influence the results of surface urban heat island studies. Moreover, the relationship between NDVI and LST is well known to be nonlinear and predominantly bare soil locations experience a wider variation in surface radiant temperature than densely vegetated locations (Carlson et al. 1994; Gillies & Carlson, 1995; Owen et al., 1998; Price, 1990). The variability and nonlinearity suggest that NDVI alone may not be a

sufficient metric to study SUHI quantitatively. To reduce the problem, Weng et al. (2004) recently proposed using the vegetation fraction within a pixel derived from a spectral mixture model instead of NDVI as a new indicator. They found that the vegetation fraction has a slightly stronger negative correlation with LST. Although the vegetation fraction differs from NDVI by making use of the full spectral reflectance vector of a sensor, it is still one type of vegetation index, and it is strongly related to NDVI (Carlson & Ripley, 1997; Gutman & Ignatov, 1998). Therefore, fractional vegetation cover suffers the same limitations of variability and nonlinearity as NDVI.

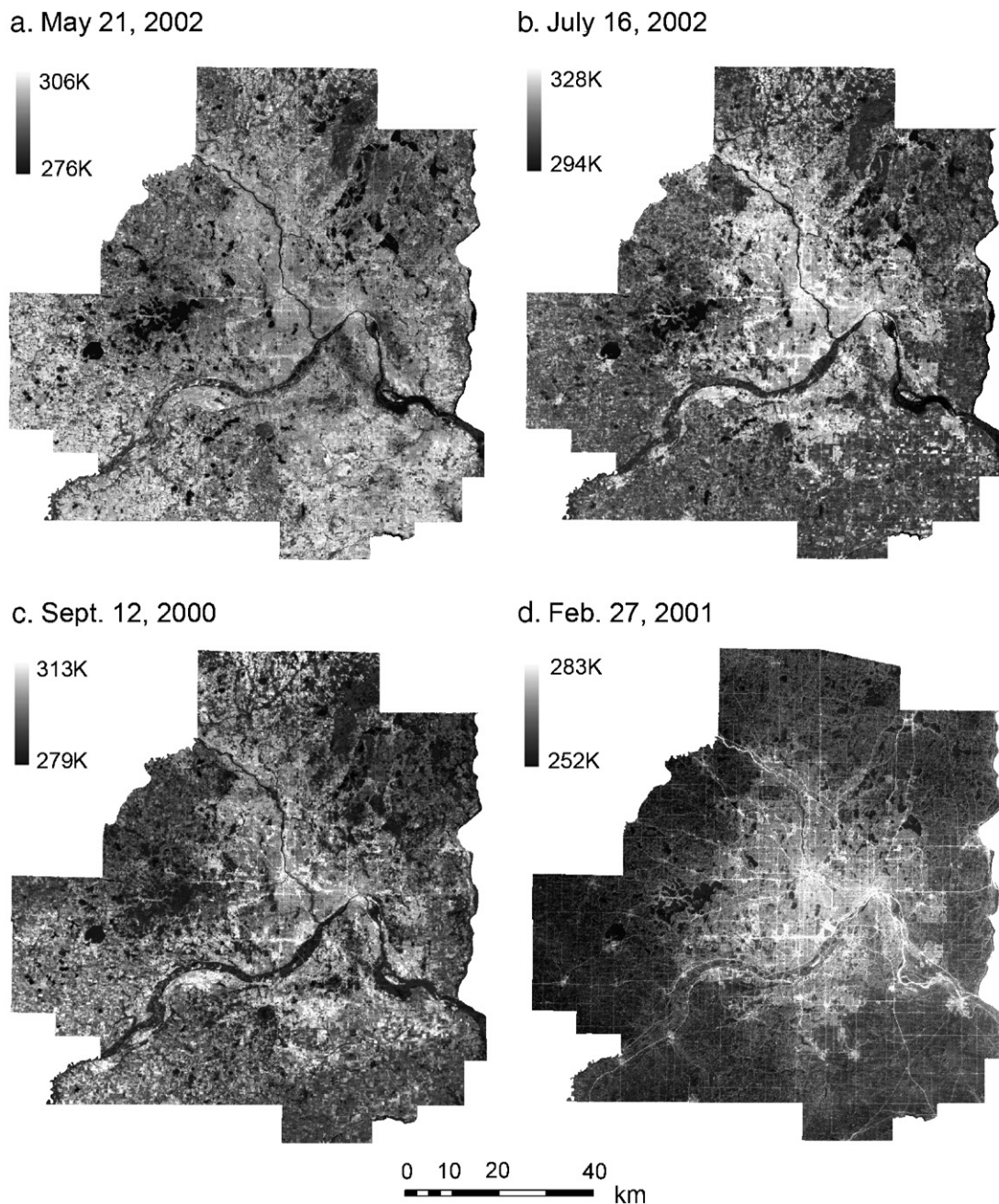


Fig. 2. LST derived from Landsat TM (b, c) and ETM+ (a, d) imagery for four different dates.

On the other hand, SUHI phenomena have been investigated by analyzing the relationship between the LST and urbanization in various urban climate studies (Arthur et al., 2000; Carlson & Arthur, 2000; Oke, 1976; Weng, 2001). In remote sensing, classifications of impervious surface area are being used to quantify and map the degree of urbanization and extent of urban land use (Bauer et al., 2004; Civco et al., 2002; Yang et al., 2003). Impervious surfaces are surfaces which water cannot infiltrate and are primarily associated with transportation (streets, highways, parking lots and sidewalks) and building rooftops. The amount of impervious surfaces is related to population growth and urbanization (Stankowski, 1972) and is an important indicator of environmental quality (Arnold & Gibbons, 1996). Therefore, analyzing the relationship between the LST and percent impervious surface area (%ISA) in an urbanized environment provides an alternative for studies of urban expansion and related surface UHI phenomena. Previous studies have shown that the higher the urban intensity or imperviousness, usually the higher the land surface temperature (Oke, 1976; Weng, 2001).

Compared to the NDVI, the %ISA is more stable and less affected by seasonal changes suggesting that %ISA may provide an additional metric for analysis of land surface temperatures and urban thermal patterns. However, comparative studies of NDVI and %ISA as indicators of surface UHI are very limited. The objective of this study was to explore and compare the relationships of LST to NDVI and %ISA using Landsat TM and ETM+ data obtained from four different seasons using Twin Cities Metropolitan Area (TCMA) as a case study.

2. Methods

2.1. Study area

The study area covers the seven-county Twin Cities Metropolitan Area (TCMA) of Minnesota, an area of approximately 7700 km². Most of the TCMA area is covered by level to rolling plains with elevation ranging from 198 to 370 m. The lowest

elevation areas are primarily associated with the Minnesota and Mississippi Rivers, while the highest elevation regions are mostly located in Lakeville, Elko, and New Market in the south central TCMA. It includes a diversity of land cover classes interspersed with over 900 lakes, thousands of wetlands, and is transected by the Minnesota, Mississippi and St. Croix Rivers. High and low density urban development characterizes the central portion and several rural land cover types of agricultural fields, grasslands, wetlands and forests characterize the surrounding landscape (Fig. 1). Our previous study (Yuan et al., 2005) showed that in 2002, approximately 33% of the total land was urban, 40% agriculture, and about 14% forest. In recent decades, a diversified and growing economy has continuously attracted new residents and stimulated significant urban growth. The population of the core seven counties — Anoka, Carver, Dakota, Hennepin, Ramsey, Scott, and Washington — grew from 2.28 to 2.64 million from 1990 to 2000. The diversity of land cover types and uses, combined with the growing urbanization in the TCMA makes it an ideal area to analyze SUHI effects.

2.2. Image pre-processing

Landsat data from four different seasons were obtained. Two Landsat-5 Thematic Mapper (TM) images (Row 29/Path 27), acquired on July 16, 2002 and September 12, 2000, and two Landsat-7 Enhanced Thematic Mapper Plus (ETM+) images, acquired on February 27, 2001 and May 21, 2002, were analyzed. Although the mid-morning timing of the Landsat overpass is not ideal for analysis of the SUHI, it is feasible without major loss of information. Nevertheless, from approximately 10:00 to 14:00, the influence of the onset time for transient water stress may affect the radiant surface temperature (Carlson et al., 1995b).

The Landsat images were rectified to the UTM projection system (ellipsoid GRS80, datum NAD83, zone 15) and were georeferenced to a Minnesota Department of Transportation base map using approximately 60 ground control points, primarily highway intersections, evenly distributed across the

Table 1
Records of National Weather Service temperature observations compared to the Landsat TM measured LST (K)

Station name	County	Lat.	Long.	Elev.	July 16, 2002				February 27, 2001			
					T_{max}	T_{min}	T_{mean}	LST	T_{max}	T_{min}	T_{mean}	LST
Cedar	Anoka	45.32	-93.28	276.5	303.1	292.6	298.1	300.8	262.6	249.2	255.9	258.3
Chanhasen WFO	Carver	44.85	-93.57	288.3	304.8	292.0	298.7	301.2	260.9	250.9	255.9	259.6
Farmington 3 NW	Dakota	44.67	-93.18	298.7	304.2	291.5	298.1	310.0	265.4	251.5	258.7	263.5
Hastings Lock 2	Dakota	44.77	-92.87	211.8	300.9	291.5	296.5	298.5	267.6	254.8	261.5	263.2
Rosemount Ag Expt Sta	Dakota	44.72	-93.10	289.6	300.9	292.0	296.5	302.9	268.1	249.8	259.2	258.7
St Paul	Ramsey	44.97	-93.03	274.3	304.8	292.6	298.7	306.2	263.1	252.6	258.1	263.5
UMN St Paul	Ramsey	44.98	-93.18	295.7	305.4	294.2	299.8	311.2	264.2	252.0	258.1	263.1
Vandais Lake	Ramsey	45.07	-93.10	271.3	305.9	288.1	297.0	301.2	265.4	245.4	255.4	260.4
Jordan 1 S	Scott	44.65	-93.62	283.5	303.1	292.0	297.6	300.2	265.4	249.8	257.6	257.9
Stillwater	Washington	45.05	-92.80	216.4	305.4	292.6	299.2	304.2	267.6	254.2	260.9	262.1
Lower St. Anthony Falls	Hennepin	44.98	-93.18	289.6	308.1	293.1	300.9	311.2	262.0	250.9	256.5	264.3
Minneapolis–St. Paul Airport	Hennepin	44.88	-93.23	265.8	305.4	294.8	300.4	312.5	262.6	253.7	258.1	263.1
New Hope	Hennepin	45.02	-93.63	309.7	305.4	293.7	299.8	300.5	263.7	252.0	258.1	258.7

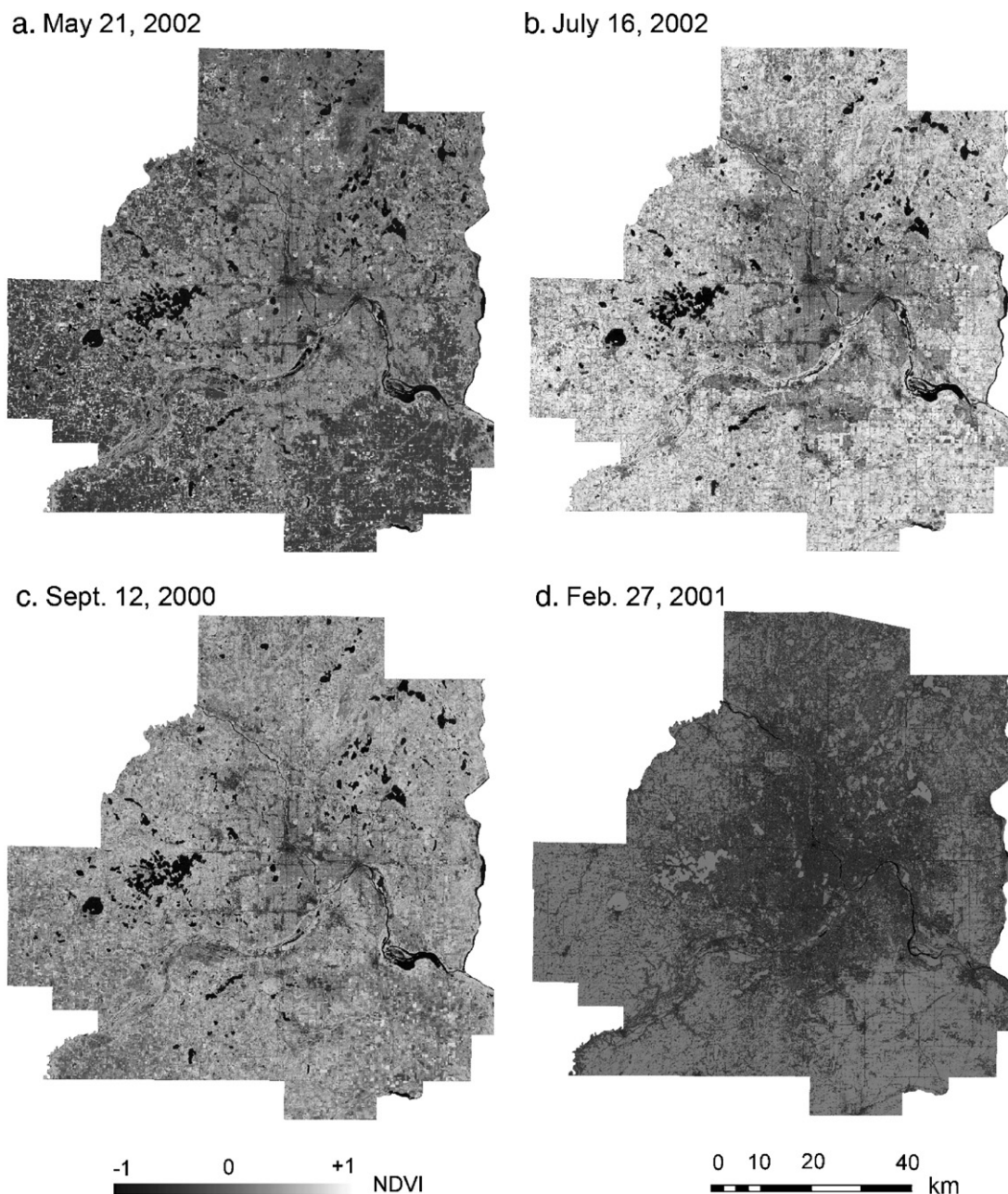


Fig. 3. NDVI derived from Landsat TM (b, c) and ETM+ (a, d) imagery for four different dates.

image. A first order polynomial model was used for the rectification with nearest neighbor resampling. The root mean square (RMS) errors were less than 0.25 pixels (7.5 m) for each of the four images. The original digital numbers (DN) of the TM and ETM+ images were converted to exo-atmospheric reflectance based on the methods provided by Chander and Markham (2003) and the Landsat 7 Science Data Users Handbook (2006).

2.3. Calculation of LST and NDVI

The TM and ETM+ thermal infrared band (10.4–12.5 μm) data were utilized to derive the LST. The following equation

was used to convert the digital numbers (DN) to space reaching radiance or top-of-atmospheric (TOA) radiance measured by the instrument (Chander & Markham, 2003):

$$L_{\lambda} = \frac{L_{\max} - L_{\min}}{\text{QCAL}_{\max} - \text{QCAL}_{\min}} (\text{DN} - \text{QCAL}_{\min}) + L_{\min} \quad (1)$$

where L_{λ} is TOA radiance at the sensor's aperture in $\text{W}/(\text{m}^2 \text{sr } \mu\text{m})$, QCAL_{\max} (=255) and QCAL_{\min} (=0) are the highest and the lowest points of the range of rescaled radiance in DN, L_{\min} and L_{\max} are the TOA radiances that are scaled to QCAL_{\min} and QCAL_{\max} in $\text{W}/(\text{m}^2 \text{sr } \mu\text{m})$.

The TOA radiance was then converted to surface-leaving radiance by removing the effects of the atmosphere in the thermal region. Specifically, an atmospheric correction tool developed by Barsi et al. (2005) and available at (<http://atmcorr.gsfc.nasa.gov/>) for the thermal band of Landsat sensors was applied. This tool uses the MODTRAN radiative transfer code and a suite of integration algorithms to estimate three parameters — atmospheric transmission and upwelling and downwelling radiance — which allows surface-leaving radiance to be calculated using Eq. (2) (Barsi et al., 2005):

$$L_T = \frac{L_\lambda - L_\mu - \tau(1-\varepsilon)L_d}{\tau\varepsilon} \quad (2)$$

where L_T is the radiance of a blackbody target of kinetic temperature T , L_λ is the space-reaching or top-of-atmospheric radiance measured by the instrument, L_μ is the upwelling or atmospheric path radiance, L_d is the downwelling or sky radiance, τ is the atmospheric transmission, and ε is the emissivity of the surface, specific to the target type. Radiances are in units of $\text{W}/(\text{m}^2 \text{ sr } \mu\text{m})$ and the transmission and emissivity are unitless. The emissivities were based on our land cover classification (Yuan et al., 2005) and emissivity values from Snyder et al. (1998). The emissivities for all the non-urban land covers of the winter image were assumed to be the same as snow.

Lastly, the radiance was converted to surface temperature using the Landsat specific estimate of the Planck curve (Eq. (3)) (Chander & Markham, 2003):

$$T = \frac{K_2}{\ln\left(\frac{K_1}{L_T} + 1\right)} \quad (3)$$

where T is the temperature in Kelvin (K), K_1 is the pre-launch calibration constant 1 in $\text{W}/(\text{m}^2 \text{ sr } \mu\text{m})$ and K_2 is the pre-launch calibration constant 2 in Kelvin. For Landsat 5 TM, $K_1=607.76 \text{ W}/(\text{m}^2 \text{ sr } \mu\text{m})$ and $K_2=1260.56 \text{ K}$; for Landsat 7 ETM+, $K_1=666.09 \text{ W}/(\text{m}^2 \text{ sr } \mu\text{m})$ and $K_2=1282.71 \text{ K}$. According to Barsi et al. (2005), with the atmospheric correction, the final apparent surface temperatures have uncertainties less than 2 K when the atmosphere is relatively clear.

Normalized difference vegetation index maps were derived for all the four images as follows:

$$\text{NDVI} = \frac{R_{\text{NIR}} - R_{\text{red}}}{R_{\text{NIR}} + R_{\text{red}}} \quad (4)$$

where R_{NIR} and R_{red} are the spectral reflectances in the TM and ETM+ red and near-infrared bands. This NDVI equation produces values in the range from -1 to 1 , where positive values

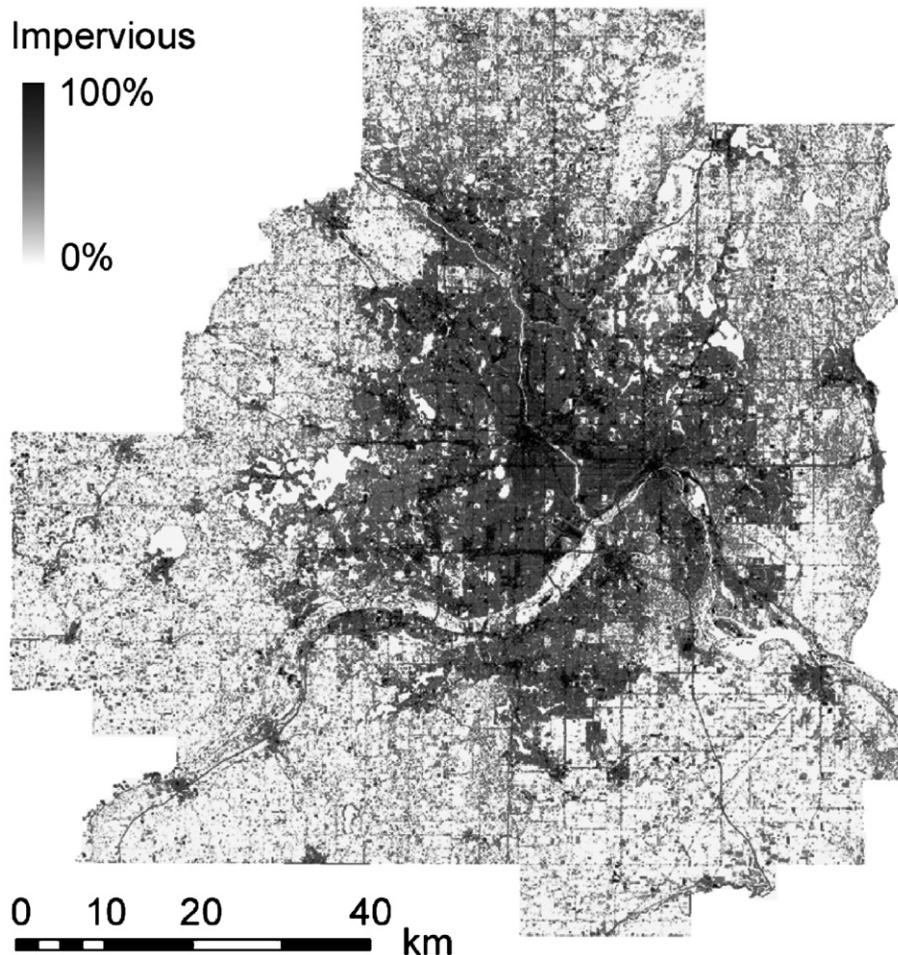


Fig. 4. Percent impervious surface classification of the TCMA for 2002.

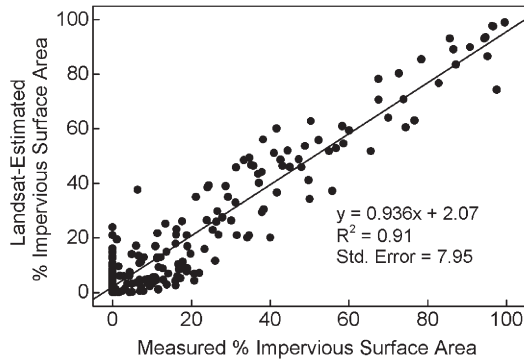


Fig. 5. Relationship of Landsat-estimated percent and DOQ-measured percent impervious surface area.

indicate vegetated areas and negative values signify non-vegetated surface features such as water, barren, clouds, and snow.

2.4. Classifications of percent impervious surface

A normalized spectral mixture analysis (NSMA) approach developed by Wu (2004) was utilized to classify the percent impervious surface by modeling a mixed spectrum as a linear combination of vegetation–impervious surface–soil (V–I–S) endmembers for the July 16, 2002 image. In his paper, Wu (2004) discussed the brightness variation problems in urban applications, and argued that shade should not be considered as an urban class, but a factor that adversely influences modeling

results since the endmember shade may not only represent a portion of actual shade but also likely be a part of vegetation, impervious surface, or soil. To address the problem, Wu (2004) proposed the NSMA, in which the normalization process reduces the variation while maintaining useful information for separating V–I–S land cover types. He reported that the three-endmember NSMA can model the heterogeneous urban composition successfully with higher accuracy than the typical four-endmember SMA models if water is masked out.

Specifically, the NSMA model starts by implementing a normalization (Eq. (5)) on the original TM/ETM+ data to reduce radiometric variations while maintaining useful information to separate major land cover types:

$$\bar{R}_b = \frac{R_b}{m} \times 100 \quad (5)$$

where $m = \frac{1}{n} \sum_{b=1}^n R_b$ and \bar{R}_b is the normalized reflectance for band b in a pixel; R_b is the original reflectance for band b ; m is the average reflectance for that pixel; and n is the total number of bands.

Next, a linear spectral mixture analysis (LSMA) was utilized to calculate the fractions of the three endmembers within the normalized spectra. Spectral mixture analysis is an advanced image processing method that determines the fraction of components contained in each pixel of an image by comparing the actual pixel spectrum with a reference library of spectra of pure components. This method has been widely used for subpixel-level land cover classifications in remote sensing

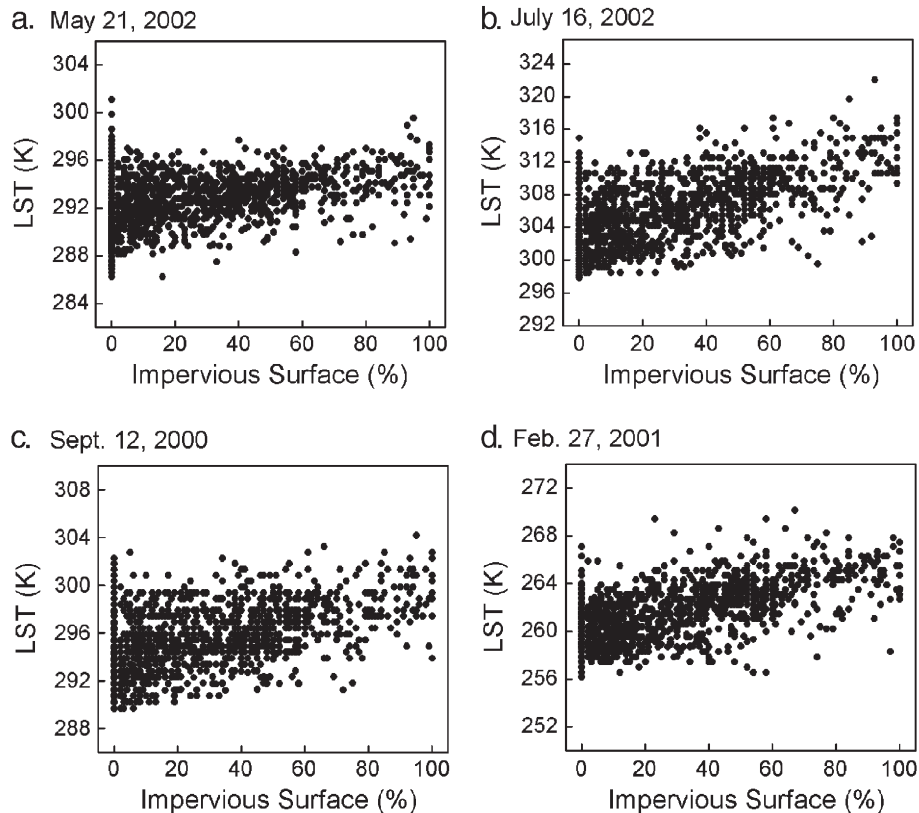


Fig. 6. Scatterplots of LST vs. percent impervious surface area for four dates.

imagery (Adams et al., 1995; Heinz & Chang, 2001; Lu et al., 2003; Lu & Weng, 2004; Phinn et al., 2002; Rashed et al., 2001; Roberts et al., 1998; Settle & Drake, 1993; Small, 2001; Weng et al., 2004; Wu, 2004; Wu & Murray, 2003). The LSMA describes the surface composition in each pixel of an image using pure land covers, so-called endmembers, and assumes a linear combination of these endmembers (Eq. (6)):

$$\bar{R}_b = \sum_{i=1}^{n'} \bar{f}_i \bar{R}_{i,b} + e_b \quad (6)$$

where $\sum_{i=1}^{n'} \bar{f}_i = 1$ and $\bar{f}_i \geq 0$; \bar{R}_b is the normalized reflectance for band b obtained from Eq. (4); $\bar{R}_{i,b}$ is the normalized reflectance of endmember i in band b ; \bar{f}_i is the fraction of endmember i ; n' is the number of endmembers; and e_b is the residual.

The fraction of each land cover type, including vegetation, impervious surface, and soil, in a pixel can be derived with a least squares method in which the residual e_b is minimized. When field or laboratory measurements are not available, endmembers can be selected from the TM/ETM+ images (Wu & Murray, 2003; Wu, 2004). In this study, clusters of each of the endmembers were identified by visual interpretation of the Landsat images and the feature space images of a principal component transformation. Further detailed information about the NSMA and justification of endmember selection can be found in Wu (2004).

The accuracy of the impervious surface map was assessed using area of interest (AOI) samples determined from 2003

National Agricultural Imagery Program (NAIP) 1-meter color digital orthoimagery. A sampling unit of 3×3 pixels was chosen to minimize the impacts of registration errors (approximately 0.25 pixels) between the Landsat and NAIP images. All impervious areas within each AOI were carefully digitized and the percent impervious surface for each AOI was calculated by dividing the area of the impervious surface polygons by the total area of the AOI. Originally 250 random samples were generated for the entire image. Samples outside of the study area were subsequently excluded, leaving 238 valid samples representing varying percentages and kinds of impervious surfaces.

3. Results and discussion

3.1. LST patterns and statistics

The digital remote sensing method provides not only a measure of the magnitude of surface temperatures of the entire metropolitan area, but also the spatial extent of the surface heat island effects (Fig. 2). The late spring LST map had a range of 276–306 K with the highest surface temperatures located in the central business district areas of Minneapolis and St. Paul and the recently planted crop fields of rural areas. The summer LST showed striking SUHI effects with urban and rural surface temperature contrasts. General patterns of SUHI with a maximum LST difference of 24 K between urban and rural areas and a mean temperature of 304 K for the entire TCMA with a spatial extent of 72 km N–S and 50 km E–W for the core

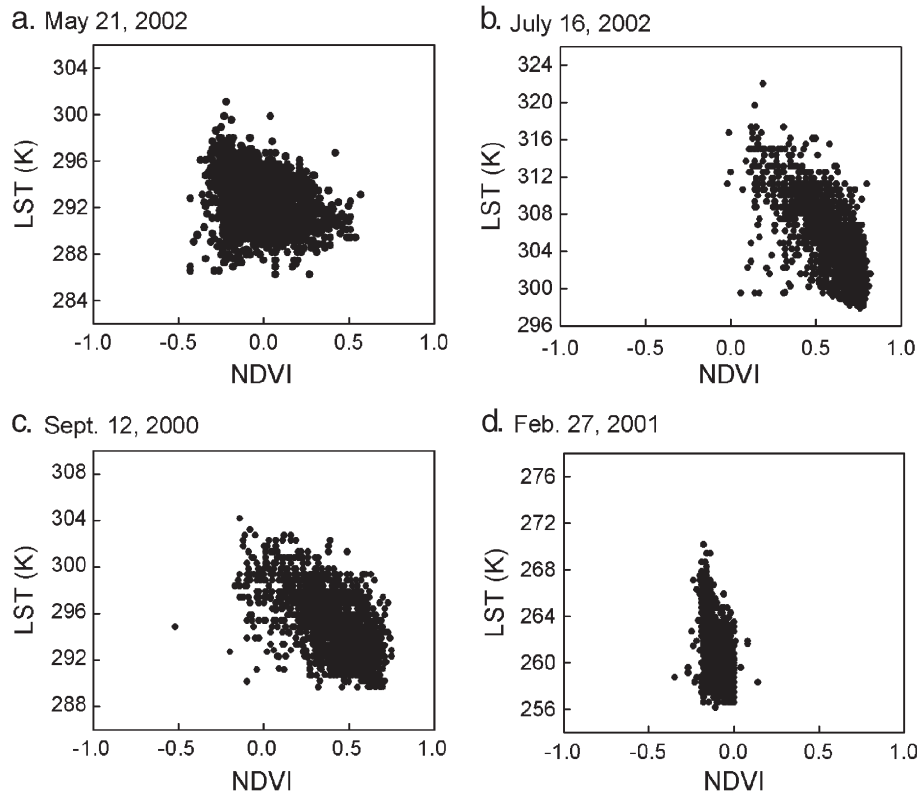


Fig. 7. Scatterplots of LST vs. NDVI for four dates.

SUHI are shown in Fig. 2b. Three apparent hot spots — Minneapolis and St. Paul downtown areas and the International Airport — can be identified. There were also clear patterns along the highway I-94 northwest of Minneapolis and along the southwestern perimeter following the Minnesota River and Highway 169. The general extent of the heat island was covered essentially by the 2010 Metropolitan Urban Service Area (MUSA) boundary, which delineates the outer reaches of the regional utility services and urban development. The September LST values displayed a range comparable to that of the May LST map, but their thermal patterns were different, especially in rural areas where vegetated surfaces had cooler temperatures than harvested fields in September. The winter LST map ranged from 252 K to 283 K, and had a mean value of 260 K (Fig. 2d). On this map, the urban center and major roads were much warmer than the rural areas covered by snow. The coolest temperatures were in the western rural part of the TCMA where urbanization is minimal. In addition, the higher spatial resolution (60 m) of the ETM+ thermal-band imagery is apparent in Fig. 2a and d when compared to the 120-meter resolution of the TM thermal-band data in Fig. 2b and c.

Air temperature data from the National Climate Data Center (NCDC) were compared to the satellite LST estimates. For our study site, 13 records of climatologic observations were extracted for the summer and winter dates (Table 1). They are distributed nearly evenly across the TCMA and each county has at least one station. The satellite-based LST was 6 K and 3 K

higher than the air temperatures for the summer and the winter dates, respectively, which is reasonable since daytime surface temperatures of dry ground are generally warmer than that of air temperature. It is also known that precise equivalence between LST and the near-ground air temperature is difficult to obtain and to estimate the surface energy fluxes over complex terrain is beyond satellite thermal sensing data's capability as the surface energy budget is too complicated (Carlson et al., 1995b). To correct the differences between satellite measured LST and the near-ground air temperature, not only concurrent in-situ ground data such as surface and soil temperatures, but also accurate models that relate the surface and air temperatures are required.

3.2. NDVI maps and impervious surface classification

NDVI maps for the four dates are shown in Fig. 3. On May 21, 2002, NDVI varied from -0.59 to 0.62 with a mean value of -0.02 ; urban grass had the highest value. This late spring NDVI map displayed lower values than the summer date when foliage was complete. While there was a large variation ($-0.32 - 0.85$), the summer NDVI had the highest average value of 0.62 among all dates. Compared to the skewed histogram of summer NDVI, the fall NDVI had an approximate normal distribution with a mean of 0.42 and standard deviation of 0.18 , indicating a clear greenness decrease from July to September. In case of winter, NDVI ranged from -0.66 to 0.48 and the majority of values were between -0.2 and 0.02 with a

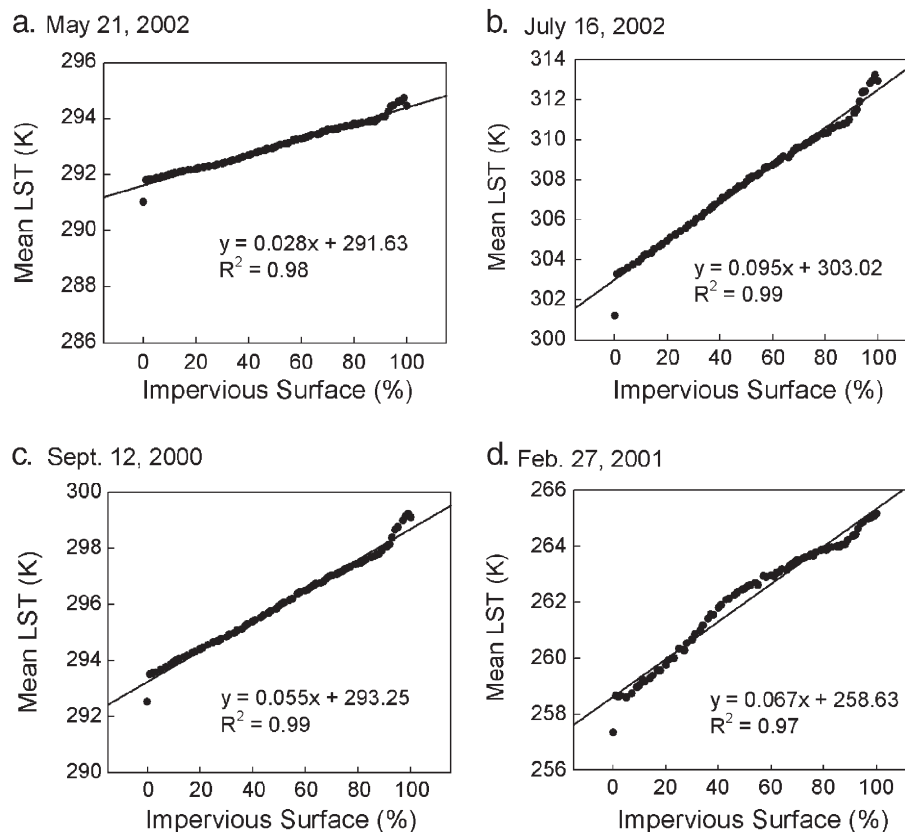


Fig. 8. Relationship of mean LST to percent impervious surface area.

mean of -0.09 . This is not surprising since nearly all of the non-impervious areas of the TCMA, except conifer forests, were covered by snow.

The percent impervious surface area from the normalized spectral mixture analysis with a continuous range of impervious area from 0–100% is mapped in Fig. 4. The detail in the classification allows one to easily locate the major highways, central business districts, urban residential areas with varying densities and patterns, and rural development centers, as well as rural undeveloped areas. The accuracy (Fig. 5) of the Landsat classification of impervious surface area was determined by comparing the Landsat-estimated ISA to the orthoimage measurements. The two measurements are highly correlated ($r^2=0.91$) with a standard error of 7.95%, indicating an accurate classification of percent impervious surface area.

3.3. LST relationships to NDVI and percent impervious surface

A sample with 3000 randomly generated points was used to investigate the relationships of LST to NDVI and percent impervious surface area. In order to facilitate the comparison, sample points located in water bodies were excluded. Fig. 6 indicates consistent linear patterns between LST and percent impervious surface for all the seasons, while in Fig. 7 the relationship between LST and NDVI is nonlinear and strongly affected by season. Research over the past two decades has shown that the surface radiant temperature response is determined by both surface soil water content and vegetation cover (Carlson et al., 1994; Gillies & Carlson, 1995; Goward

et al., 1985; Nemani & Running, 1989; Owen et al., 1998; Price, 1990; Weng et al., 2004).

In the urbanized area of the study site where bare soil is limited, LST measurements typically represent the radiometric temperatures of vegetated and non-vegetated surfaces, mainly impervious surfaces. Given the pixel sizes of 120 and 60 m in Landsat TM and ETM+ thermal imagery, the resultant temperatures depend on the relative proportions of surfaces. The variation in the pixel temperatures may be mostly related to impervious surface amounts and characteristics since vegetated surfaces vary less in temperature than sunlit impervious surfaces. This explains the linear pattern between LST and imperviousness in the scatterplots of Fig. 6. By contrast, as shown in Fig. 7a, a scatterplot of spring NDVI and LST resulted in a triangular-shaped envelope of pixels. Conversely, an irregular and highly compacted pattern with low NDVI values is shown in the scatterplot for the winter image. The corresponding figures for the summer and fall dates have similar linear patterns. These results suggest that although NDVI may be used for analysis of surface UHI effects during summer and early autumn, percent imperviousness is suitable for LST studies for all the seasons across our study site.

To further investigate these relationships, a zonal analysis was utilized to evaluate the mean LST at each 1% increment of %ISA from 0% to 100%, and at each 0.01 increment of the NDVI from -1 to 1 . A very strong linear relationship ($r^2 > 0.97$) is shown between the mean LST and percent imperviousness for all the four dates (Fig. 8), suggesting the variations in LST can be accounted for very well by %ISA for all four seasons.

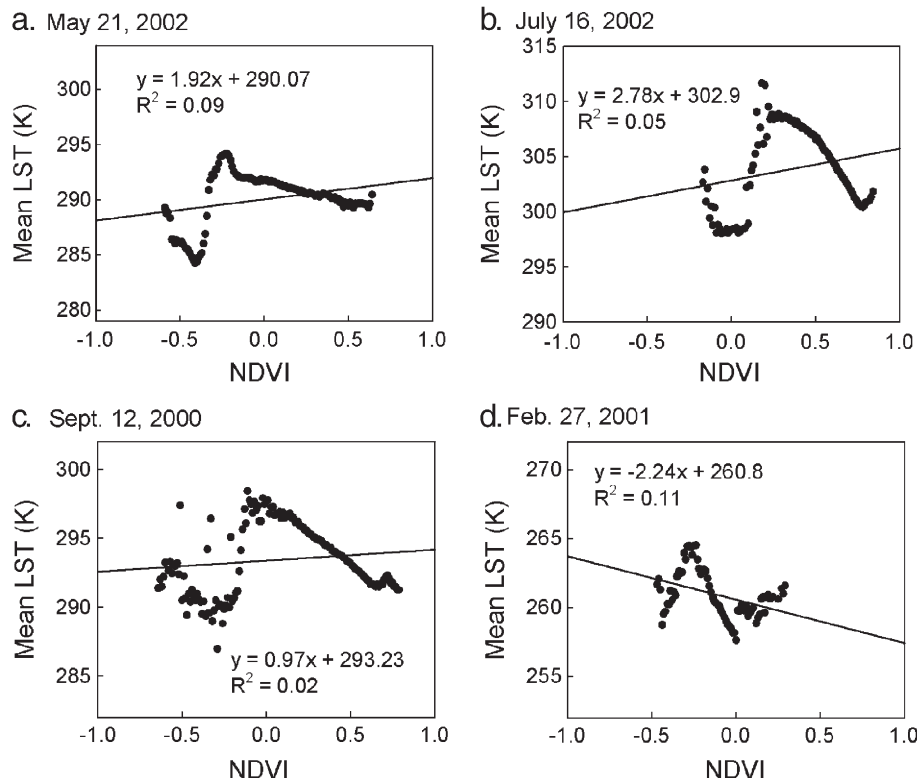


Fig. 9. Relationship of mean LST to NDVI.

The steepest slope of the linear correlation was found in the summer image, indicating that the magnitude of SUHI reaches highest in the summer. Comparatively, the lowest level of urban–rural LST difference was found in the spring image because of the high incidence of exposed dark soils. In addition, there is an evident 1–2 K mean LST gap, especially for the summer date, between the 0%ISA zone representing the pure rural areas and the 1%ISA zone of areas with the smallest amount of urbanization.

On the other hand, the associations between the mean LST and NDVI graphed in Fig. 9 are not straightforward. Specifically, in the first three graphs (Fig. 9a–c), it appears there are at least two different areas: when $NDVI < -0.1$ for May and September imagery and < 0.1 for July imagery (which represents heterogeneous effects from diverse non-vegetated areas of high density urban surfaces, non-vegetated wetland, and bare soil), no stable trend that can be identified. By contrast, at higher NDVI values there is an inverse linear association with some variations at the highest NDVI levels on all three graphs, indicating there is a negative correlation between NDVI and LST from late spring to fall. However, the relationship tends to break down in the rural surroundings outside of the city. Compared to the other three dates the winter maps (Figs. 3d and 9d) look very different with no evident association between the SUHI and the NDVI, which further implies using NDVI to understand SUHI is complicated since NDVI itself suffers strong seasonal changes. Conversely, the %ISA reflects seasonal SUHI fluctuations in similar linear patterns, but with different intercepts and slopes, which makes it a useful tool for analysis and understanding of multitemporal SUHI effects.

4. Conclusions

The study investigated the relationships between the LST, %ISA, and NDVI in the seven-county Twin Cities metropolitan area. Results indicate %ISA is an accurate indicator of SUHI effects with strong linear relationships between LST and %ISA for all the four seasons, whereas the relationship between LST and NDVI suffers from evident seasonal changes and it is better restricted to analysis of SUHI effects during summer and early autumn. The strong linear relationship model between the LST and %ISA suggests that impervious surface area accounts for most of the variation in land surface temperature dynamics. This implies that %ISA can be used as a complementary metric to the traditionally applied NDVI for analyzing LST quantitatively over the seasons for surface urban heat island studies. While we found the variations in surface temperature can be better accounted for by differences in imperviousness than by the commonly used NDVI, we also realize that the conclusion is based on only one area and four different dates. Although the overpass time and 16-day revisit interval of Landsat are not ideal for dynamic surface heat island analysis, the data nevertheless provide useful information for measuring and understanding urban heat island effects. Further studies of additional metropolitan areas and different satellite data such as MODIS are recommended.

Acknowledgements

The support of the Department of Geography, Minnesota State University, Mankato and the Department of Forest Resources and Agricultural Experiment Station (project MN-42-037), University of Minnesota, is gratefully acknowledged. Many thanks also go to all the reviewers for their constructive comments and suggestions.

References

- Adams, J. B., Sabol, D. E., Kapos, V., Almeida-Filho, R., Roberts, D. A., Smith, M. O., et al. (1995). Classification of multiple images based on fractions of endmembers: Application to land-cover change in the Brazilian Amazon. *Remote Sensing of Environment*, 52, 137–154.
- Arnold, C. L., & Gibbons, C. J. (1996). Impervious surface coverage: The emergence of a key environmental indicator. *Journal of the American Planning Association*, 62(2), 243–258.
- Arthur, S. T., Carlson, T. N., & Ripley, D. A. J. (2000). Land use dynamics of Chester County, Pennsylvania, from a satellite remote sensing perspective. *Geocarto International*, 15(1), 25–35.
- Barsi, J. A., Schott, J. R., Palluconi, F. D., & Hook, S. J. (2005). Validation of a web-based atmospheric correction tool for single thermal band instruments. *Proceedings, SPIE*, vol. 5882. Paper 58820E. Bellingham, WA. 7 pp.
- Bauer, M. E., Heinert, N. J., Doyle, J. K., & Yuan, F. (2004). Impervious surface mapping and change monitoring using satellite remote sensing. *Proceedings, American Society of Photogrammetry and Remote Sensing Annual Conference*. May 24–28, 2004. unpaginated CD ROM, 10 pp.
- Carlson, T. N., & Arthur, S. T. (2000). The impact of land use/land cover changes due to urbanization on surface microclimate and hydrology: A satellite perspective. *Global and Planetary Change*, 25, 49–65.
- Carlson, T. N., & Ripley, D. A. (1997). On the relation between NDVI, fractional vegetation cover, and leaf area index. *Remote Sensing of Environment*, 62, 241–252.
- Carlson, T. N., Gillies, R. R., & Perry, E. M. (1994). A method to make use of thermal infrared temperature and NDVI measurements to infer surface soil water content and fractional vegetation cover. *Remote Sensing Reviews*, 9, 161–173.
- Carlson, T. N., Gillies, R. R., & Schmugge, T. J. (1995a). An interpretation of methodologies for indirect measurement of soil water content and fractional vegetation cover. *Agricultural and Forest Meteorology*, 77, 191–205.
- Carlson, T. N., Taconet, O., Vidal, A., Gillies, R. R., Olioso, A., & Humes, K. (1995b). An overview of the workshop on thermal remote sensing held at La Londe les Maures, France, September 20–24, 1993. *Agricultural and Forest Meteorology*, 77(3), 141–151.
- Chander, G., & Markham, B. (2003). Revised Landsat-5 TM radiometric calibration procedures and postcalibration dynamic ranges. *IEEE Transactions on Geoscience and Remote Sensing*, 41(11), 2674–2677.
- Civco, D. L., Hurd, J. D., Wilson, E. H., Arnold, C. L., & Prisloe Jr., M. P. (2002). Quantifying and describing urbanizing landscapes in the northeast United States. *Photogrammetric Engineering and Remote Sensing*, 68(10), 1083–1090.
- Gallo, K. P., McNab, A. L., Karl, T. R., Brown, J. F., Hood, J. J., & Tarpley, J. D. (1993). The use of NOAA AVHRR data for assessment of the urban heat island effect. *Journal of Applied Meteorology*, 32(5), 899–908.
- Gallo, K. P., & Owen, T. W. (1999). Satellite based adjustments for the urban heat island temperature bias. *Journal of Applied Meteorology*, 38, 806–813.
- Gillies, R. R., & Carlson, T. N. (1995). Thermal remote sensing of surface soil water content with partial vegetation cover for incorporation into climate models. *Journal of Applied Meteorology*, 34, 745–756.
- Gillies, R. R., Carlson, T. N., Cui, J., Kustas, W. P., & Humes, K. S. (1997). A verification of the ‘triangle’ method for obtaining surface soil water content and energy fluxes from remote measurements of the Normalized Difference Vegetation Index (NDVI) and surface radiant temperature. *International Journal of Remote Sensing*, 18, 3145–3166.

- Goward, S. N., Cruickshank, G. D., & Hope, A. S. (1985). Observed relation between thermal emission and reflected spectral radiance of a complex vegetated landscape. *Remote Sensing of Environment*, 18, 137–146.
- Goward, S. N., Xue, Y., & Czajkowski, K. P. (2002). Evaluating land surface moisture conditions from the remotely sensed temperature/vegetation index measurements: an exploration with the simplified simple biosphere model. *Remote Sensing of Environment*, 79, 225–242.
- Gutman, G., & Ignatov, A. (1998). The derivation of the green vegetation fraction from NOAA/AVHRR data for use in numerical weather prediction models. *International Journal of Remote Sensing*, 19(8), 1533–1543.
- Heinz, D. C., & Chang, C. I. (2001). Fully constrained least-squares linear spectral mixture analysis method for material quantification in hyperspectral imagery. *IEEE Transactions on Geoscience and Remote Sensing*, 39(3), 529–545.
- Landsat 7 Science Data Users Handbook, 2006. URL: http://ftpwww.gsfc.nasa.gov/IAS/handbook/handbook_toc.html, National Aeronautics and Space Administration (last date accessed 10 August 2006).
- Lo, C. P., Quattrochi, D. A., & Luvall, J. C. (1997). Application of high-resolution thermal infrared remote sensing and GIS to assess the urban heat island effect. *International Journal of Remote Sensing*, 18, 287–304.
- Lu, D., Moran, E., & Batistella, M. (2003). Linear mixture model applied to Amazonian vegetation classification. *Remote Sensing of Environment*, 87, 456–469.
- Lu, D., & Weng, Q. (2004). Spectral mixture analysis of the urban landscape in Indianapolis city with Landsat ETM+ imagery. *Photogrammetric Engineering and Remote Sensing*, 70(9), 1053–1062.
- Nemani, R. R., & Running, S. W. (1989). Estimation of regional surface resistance to evapotranspiration from NDVI and Thermal-IR AVHRR data. *Journal of Applied Meteorology*, 28, 276–284.
- Oke, T. R. (1976). City size and the urban heat island. *Atmospheric Environment*, 7, 769–779.
- Oke, T. R. (1982). The energetic basis of the urban heat island. *Quarterly Journal of the Royal Meteorological Society*, 108, 1–24.
- Owen, T. W., Carlson, T. N., & Gillies, R. R. (1998). An assessment of satellite remotely-sensed land cover parameters in quantitatively describing the climatic effect of urbanization. *International Journal of Remote Sensing*, 19, 1663–1681.
- Phinn, S., Stanford, M., Scarth, P., Murray, A. T., & Shyy, T. (2002). Monitoring the composition and form of urban environments based on the vegetation–impervious surface–soil (VIS) model by sub-pixel analysis techniques. *International Journal of Remote Sensing*, 23(20), 4131–4153.
- Price, J. C. (1990). Using spatial context in satellite data to infer regional scale evapotranspiration. *IEEE Transactions on Geoscience and Remote Sensing*, 28, 940–948.
- Rashed, T., Weeks, J. R., & Gadalla, M. S. (2001). Revealing the anatomy of cities through spectral mixture analysis of multispectral satellite imagery: A case study of the greater Cairo region, Egypt. *Geocarto International*, 16(4), 5–15.
- Roberts, D. A., Gardner, M., Church, R., Ustin, S., Scheer, G., & Green, R. O. (1998). Mapping chaparral in the Santa Monica Mountains using multiple endmember spectral mixture models. *Remote Sensing of Environment*, 65, 267–279.
- Roth, M., Oke, T. R., & Emery, W. J. (1989). Satellite-derived urban heat islands from three coastal cities and the utilization of such data in urban climatology. *International Journal of Remote Sensing*, 10, 1699–1720.
- Settle, J. J., & Drake, N. A. (1993). Linear mixing and the estimation of ground cover proportions. *International Journal of Remote Sensing*, 14, 1159–1177.
- Small, C. (2001). Estimation of urban vegetation abundance by spectral mixture analysis. *International Journal of Remote Sensing*, 22, 1305–1334.
- Snyder, W. C., Wan, Z., Zhang, Y., & Feng, Y. Z. (1998). Classification based emissivity for land surface temperature measurement from space. *International Journal of Remote Sensing*, 19, 2753–2774.
- Stankowski, S. J. (1972). Population density as an indirect indicator of urban and suburban land-surface modifications. *Professional Paper: Report 800B*. (pp. B219–B224). U.S. Geological Survey.
- Voogt, J. A., & Oke, T. R. (2003). Thermal remote sensing of urban areas. *Remote Sensing of Environment*, 86, 370–384.
- Weng, Q. (2001). A remote sensing–GIS evaluation of urban expansion and its impact on surface temperature in the Zhujiang Delta, China. *International Journal of Remote Sensing*, 22(10), 1999–2014.
- Weng, Q., Lu, D., & Schubring, J. (2004). Estimation of land surface temperature–vegetation abundance relationship for urban heat island studies. *Remote Sensing of Environment*, 89, 467–483.
- Wu, C. (2004). Normalized spectral mixture analysis for monitoring urban composition using ETM+ imagery. *Remote Sensing of Environment*, 93(4), 480–492.
- Wu, C., & Murray, A. T. (2003). Estimating impervious surface distribution by spectral mixture analysis. *Remote Sensing of Environment*, 84, 493–505.
- Yang, L., Huang, C., Homer, C. G., Wylie, B. K., & Coan, M. J. (2003). An approach for mapping large-area impervious surfaces: Synergistic use of Landsat 7 ETM+ and high spatial resolution imagery. *Canadian Journal of Remote Sensing*, 29(2), 230–240.
- Yuan, F., Sawaya, K. E., Loeffelholz, B. C., & Bauer, M. E. (2005). Land cover mapping and change analysis in the Twin Cities Metropolitan Area with Landsat remote sensing. *Remote Sensing of Environment*, 98(2–3), 317–328.